Received: 15 December 2021 | Revised: 24 March 2022 | Accepted: 27 March 2022

DOI: 10.1111/ffe.13705

SPECIAL ISSUE ARTICLE

FFEMS Fatigue & Fracture of Engineering Materials & Structures WILEY

Characterisation of the crack tip plastic zone in fatigue via synchrotron X-ray diffraction

Manuel Carrera[1,2] | **Alejandro S. Cruces**[1] | **Joseph F. Kelleher**[3] | **Yee-Han Tai**[4] | **John R. Yates**[5] | **Philip J. Withers**[6] | **Pablo Lopez-Crespo**[1]

[1]Department of Civil and Materials Engineering, University of Malaga, Malaga, Spain

[2]Bettergy SL, Malaga, Spain

[3]ISIS, Rutherford Appleton Laboratory, Didcot, UK

[4]Rolls-Royce plc, Derby, UK

[5]Sheffield Fracture Mechanics, Derbyshire, UK

[6]Henry Royce Institute, Department of Materials, University of Manchester, Manchester, UK

Correspondence
Alejandro S. Cruces and Pablo Lopez-Crespo, Department of Civil and Materials Engineering, University of Malaga, Malaga 29071, Spain.
Email: ascruces@uma.es and plopezcrespo@uma.es

Funding information
Engineering and Physical Sciences Research Council, Grant/Award Numbers: EP/R00661X/1, EP/S019367/1, EP/P025021/1, EP/P025498/1; European Social Found, Grant/Award Number: UMAJI84; Programa Operativo FEDER (Junta de Andalucia, Spain), Grant/Award Number: UMA18-FEDERJA-250; Funding for open access charge: Universidad de Málaga / CBUA

Abstract

This paper describes a new methodology for characterising the plastic zone ahead of a fatigue crack. This methodology is applied to a set of experimental data obtained by synchrotron X-ray diffraction on a bainitic steel compact tension specimen. The methodology is based on generating the equivalent Von Mises strain field from the X-ray experimental elastic strain maps. Based on the material response, a threshold is then applied on the equivalent strain maps to identify the size and shape of the plastic zone. The experimental plastic zone lies between the plane strain and plane stress Westergaard's bounds but closer to the plane strain theoretical prediction confirming that the volume analyzed is predominantly subjected to plane strain conditions. However, the observed plastic zone has a somewhat flatter shape, extending further from the crack plane but less extended in the crack growing direction.

KEYWORDS

bainitic steel, fatigue plastic zone, synchrotron X-ray diffraction

1 | INTRODUCTION

When analyzing fatigue crack development, it is common to resort to elastic fracture mechanics through the use of the stress intensity factor. Its application is widespread in both academic and industrial studies.[1] However, there are several other parameters that are more suitable to incorporate the plasticity effect at the crack tip. The J-integral or crack tip opening displacement (CTOD) is proposed as a standardized way to describe the permanent damage that occurs at the crack tip.[2] Furthermore, there are other parameters that consider the significance

of plasticity at the crack front that are perhaps less well-known and applied. For instance, opening mode and shear mode plastic intensity factors (ρ_I and ρ_{II}, respectively) characterise the elastoplastic behaviour in the crack tip area at a global scale.[3] They can be used as a complement to stress intensity factors (K_I and K_{II}), providing a rapid and efficient modeling of fatigue plasticity near the crack tip.[4] Likewise, the Christopher–James–Patterson (CJP) approach formulates two new terms to model the stresses induced by the existence of the plastic zone and to define the concept of crack as a plastic inclusion in an elastic body.[5] These are the interfacial shear stress intensity factor, K_S, and the retarding stress intensity factor, K_R. Previously, these have been computed from photoelastic data[6] and from digital image correlation data (DIC)[7] to integrate the plasticity around the crack tip into a fatigue crack growth analysis. More recently, estimation of the plastic component in CTOD ($CTOD_{plastic}$) has been recognized as a natural development of CTOD to quantify the damage taking place at the crack tip. The $CTOD_{plastic}$ parameter has a physical meaning of its own and can be measured directly.[8,9] The methodology allows simple modeling of the fatigue crack propagation behaviour in different aluminum alloys[10] and 304 L stainless steel.[11]

These parameters highlight the prominent role of the plasticity at the crack tip on the fatigue crack propagation of metals.[12] A preliminary description of the plastic zone is contained within Irwin and Dugdale's models, based on the application of a specific deformation criteria on the stress distribution around the crack tip.[2,13] Hutchinson[14] subsequently generalized these solutions under plane stress and plane strain conditions, both near and far from the crack tip itself. Figure 1A illustrates the classical evolution of the plastic zone from plane stress to plane strain conditions. A number of works make use of linear elastic fracture mechanics (LEFM) and the previously described concepts to further investigate the plastic zone (see, e.g., previous studies[14,15]). A concise and clear summary of the key models was published by Kujawski and Ellyin.[16] Later studies have dealt with the effect that the surrounding conditions have on the size and shape of the plastic region. For example, Banerjee[17] reported the impact of the specimen geometry on the size of the yielded area, noting the effect that the thickness constraint generates on the permanently deformed volume. Park[18] investigated the relation between sample thickness, crack growth rate, and the plastic zone in a 304 stainless steel and for Inconel 718. Liu[19] proposed a model for uniting both the long and physically short crack behaviours under one single model. Material influence and properties, as well as specimen loading conditions, were subsequently tested for certain anisotropic and orthotropic materials, providing an analytical

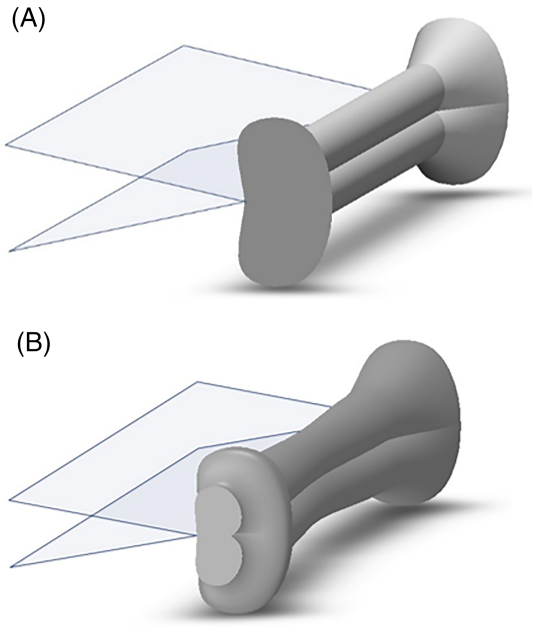

FIGURE 1 Different models of plastic zone shapes extracted from literature: (A) plastic zone shape obtained from analytical models of plane strain and plane stress boundaries and (B) evolution of the plastic zone along the surface based on ultrafine 3D finite element model (FEM) modeling (adapted from Camas et al.[22]) [Colour figure can be viewed at wileyonlinelibrary.com]

solution that quantified the relationship of load and crack angle to the plastic zone in plane strain.[20] Others have discussed the influence of Poisson's ratio and anisotropy on the crack tip plasticity, both under plane stress and plane strain conditions.[21]

The most detailed studies on fatigue crack tip plastic zone have been developed using the finite element method. For instance, Paul and Tarafder[23] identified the cyclic and monotonic plastic zone numerically, in a C-Mn grade 6 steel SA333, observing how permanent deformations were accumulated in the plastic region. Some early 2D finite element models (FEM) investigated the effect on various materials at different loading levels, relating the size of the plastic zone to crack closure effects.[24] Subsequent 2D FEM models allowed the characterisation of the plastic zone for various load magnitudes and crack lengths.[25] The validation of these FEM results was made by comparison with experimental crack growth rates. More recently, some ultrafine 3D FEM meshing has been developed to explore the size and shape of the plastic zone for various thicknesses.[26] Camas et al.[22] modeled the crack development in a 2024T3 aluminum sample by FEM and subsequently validated the results with surface DIC measurements. Those ultrafine 3D FEM results suggest a complex transition from plane stress to plane strain conditions, where the largest plastic

zone takes place at a distance from the surface (see Figure 1B). Similar results were obtained on 2024 aluminum alloy,[27] on Q370qE steel,[28] and on API 5L X80 high strength pipeline steel.[29] The transition in the plastic zone between the surface and the bulk was found to depend on parameters such as the specimen thickness and the maximum load.[30] The previous techniques cannot provide direct experimental data on the behaviour within the bulk of the material. High-energy X-ray techniques such as diffraction and computed tomography (CT) can provide direct information of the strain and the morphology deep inside the material.[31] Steuwer et al.[32] and Croft et al.[33] were among the earliest authors to obtain such high detailed data for a growing crack in an Al-Li alloy, similar to AA 5091. Results obtained by tomography and X-ray diffraction were instrumental in validating earlier FEM data for the first time. Such diffraction methods have been useful to estimate the midplane stress intensity factor of a bainitic steel sample with different elastic models.[34] An extension of this methodology towards understanding the effect of overloads was carried out by Steuwer et al.[35] who measured the residual stresses both upstream and downstream from the crack tip just after an overload event. Lopez-Crespo and co-authors[36] further examined how the plastic zone is related to the hardening of the material based on high-resolution strain maps obtained from X-ray diffraction measurements. More recently, the retardation mechanisms that occur after an overload have been identified and quantified through this technique.[37,38] Davidson et al.[39] employed several high-energy techniques such as electronic channeling contrast and X-ray microbeam to provide measurements of the microscopic properties within the plastic zone. These techniques have been proven to be of particular significance in understanding the crack closure phenomenon. For Example through the analysis of crack growth and grain orientation in an aluminum 2024.[40] Work by Barabash et al.[41] on crack closure provides another example demonstrating the effectiveness of diffraction techniques to assess the interior of samples. In this case, diffraction was used to measure the residual stress distribution around a fatigue crack tip caused by an overload. Other work by some of the current authors have addressed the topic from different perspectives. For example, the shape of the plastic zone was investigated numerically based on ultrafine 3D FEMs with an emphasis on the crack front curvature[22] and the evolution through-thickness.[26] Synchrotron X-ray diffraction data have been used to quantify the overload effect during fatigue crack growth,[36] to identify the zone of influence of an overload cycle[34] as well as to evaluate the stress intensity factor and characterise the crack tip fields in the bulk of materials.[34,42] More recently, the size and shape of the plastic zone in fatigue have been characterised for a 2024 aluminum alloy using a simpler methodology based on microindentation.[43]

In summary, there exists a number of experimental techniques for characterising the plasticity at the tip of a fatigue crack. Nevertheless, these are mostly surface techniques and cannot infer information of the plastic behaviour in the bulk of the material. The bulk of the material has been studied with 3D FEM simulations or with synchrotron X-ray techniques capable of going through the bulk of metallic materials. Given the very high computational cost of 3D FEM simulations, accurate tridimensional results on fatigue cracks have only be developed in the last 10 years or so.[26,27,29,30] Thorough validation of 3D FEM results is still lacking since most 3D simulations have either not been experimentally validated[44–49] or the validation has been based on limited surface information.[22,26–28,50] On the other hand, synchrotron X-ray radiation has been used to infer some crack properties in the bulk[35,37,38,51,52] but no direct measurement of the crack tip plastic zone has yet been achieved. The current work shows a new methodology for extracting the plastic zone created by a fatigue crack deep inside the material. To date, there is no technique other than synchrotron X-ray diffraction, capable of providing accurate experimental information about the strain distribution in the inside of the material in a nondestructive fashion. This is the first time that such a technique is used to infer the plastic zone ahead of a fatigue crack. First, the material and the fatigue test are reported. Then the synchrotron X-ray diffraction arrangement is described. Next, the methodology for estimating the plastic zone within then bulk of the material is outlined. Finally, the results are presented and discussed for three different crack configurations and the main conclusions are drawn.

2 | MATERIALS AND METHODS

2.1 | Material and fatigue test

The investigation described in this paper has been performed on a hardened and annealed bainitic steel specimen, similar to Q1N (HY80).[53] Its chemical composition is given in Table 1.

The material exhibits the following mechanical properties, as obtained from a tensile test: Young's modulus $E = 220$ GPa, yield strength $\sigma_y = 699$ MPa, and ultimate tensile strength $\sigma_u = 858$ MPa. The tensile test curve is presented in Figure 2. A Ramberg–Osgood fitting has been performed to model the experimental data (Equation 1).

TABLE 1 Composition of bainitic steel Q1N (HY80), expressed in mass %

C	Si	Mn	P	S	Cr	Ni	Mo	Cu
0.16%	0.25%	0.31%	0.01%	0.008%	1.42%	2.71%	0.41%	0.10%

Note: The balance element is Fe.

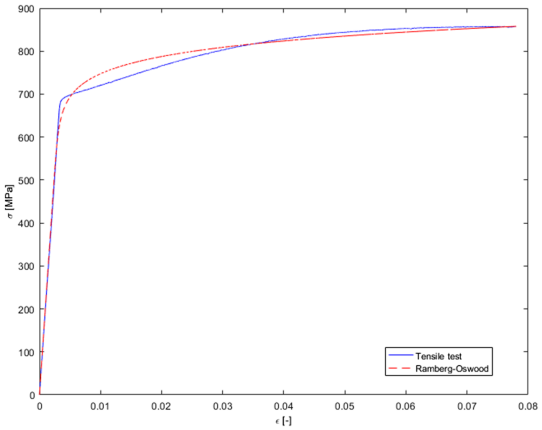

FIGURE 2 Tensile test obtained for a bainitic steel similar to Q1N (HY80) alongside the Ramberg–Osgood fit [Colour figure can be viewed at wileyonlinelibrary.com]

$$\varepsilon = \frac{\sigma}{E} + \left(\frac{\sigma}{K}\right)^n \tag{1}$$

The least squares fitting provided the following Ramberg–Osgood parameters: $K =$ 994.50 MPa and $n =$ 17.61, according to Equation 1. The Ramberg–Osgood approach is needed to model the material behaviour as a continuous function, thus increasing computational efficiency for the algorithm employed in this research.

A compact tension (CT) specimen with dimensions $W =$ 50 mm and $B =$ 12 mm was produced from this material. The specimen was precracked by applying 30,000 loading cycles, at 10 Hz frequency, the stress intensity factor range being $\Delta K =$ 28 MPa$\sqrt{\text{m}}$, and the load ratio $K_{min}/K_{max} = 0.03$. Three different fatigue stages at three different crack lengths were studied. A number of challenges and difficulties that took place during the synchrotron experiment motivated the uneven crack length distribution for the three fatigue stages. The identification of the specimens and their crack lengths is shown in Table 2.

2.2 | X-ray diffraction configuration

Synchrotron X-ray diffraction was used to measure the elastic strain on ID15 beamline at the European Synchrotron Radiation Facility (ESRF) in Grenoble (France). The experimental arrangement was similar to that described in reference.[35] Energy dispersive mode was employed with scattering angle $2\theta = 5°$ on two solid-state detectors, one horizontally and one vertically off-set, for measuring strain information in the crack growing and crack opening directions, respectively. Figure 3 shows a photograph of the experimental setup with the main elements labelled. Unlike most fatigue experiments, the loading rig was positioned horizontally (see Figure 3), which meant that the crack pointed upwards.[54] This configuration was required given the fixed position of the incoming X-ray in the beamline. A beam aperture of 60 × 60 μm was set, so that the lateral resolution was 60 μm on both horizontal and vertical directions. Such a high spatial resolution is required to capture the large strain gradients taking place around the crack tip and was achieved successfully thanks to the very small grain size of the material.[55] Larger grains introduce poor statistical sampling of the strain field increasing the point-to-point scatter.[33,56] The diffraction geometry allowed measurement of 1.4 mm long gauge volumes through the sample thickness (see Figure 4)[57] Special care was taken to control the sample position in such a way that the volume measured was at the midpoint of the sample thickness, ensuring measurements are representative of the interior state. This was achieved by taking X-ray line scans from the region of interest to the edge of the specimen and using that edge as a reference. The 2D strain field around the crack tip included information of around 500 data points collected in the neighboring of the crack tip at different fatigue stages.

TABLE 2 Crack length of the fatigue stages examined

Stage ID	FS1	FS2	FS3
a(mm)	22.0	22.1	23.9

Since the measured volume includes information over a depth of 1.4 mm along the 12 mm thickness direction, it is reasonable to assume that data obtained from the X-ray test are under predominantly plane strain conditions.[26] That is, the volume of material that is sampled is predominantly under plane strain conditions, even though the rest of the specimen might be subjected to a slightly different stress state.

The widest portion of the measured volume is located precisely at the midplane of the specimen (see Figure 4).

A grid of significant points was generated with the data obtained by averaging the strain data over the

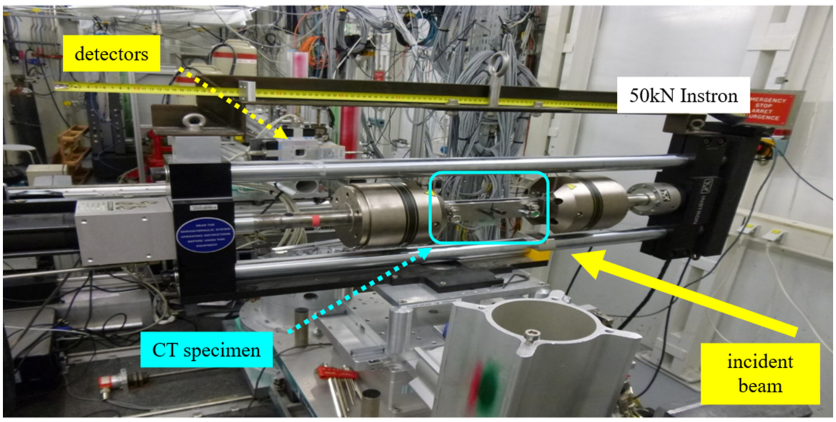

FIGURE 3 Experimental setup of the X-ray diffraction test [Colour figure can be viewed at wileyonlinelibrary.com]

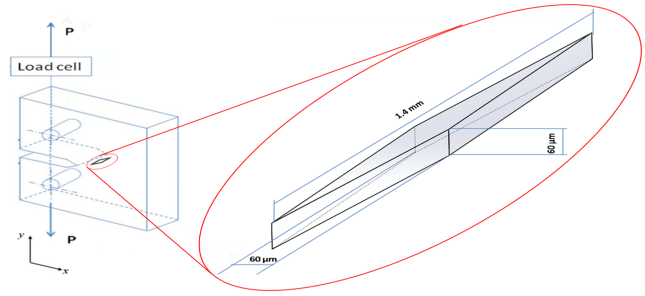

FIGURE 4 Diagram of the volume over which the strain is sampled by X-ray diffraction for each data point [Colour figure can be viewed at wileyonlinelibrary.com]

volume. Strain data were measured on the basis of an orthogonal system, along the crack growing and crack opening directions. An illustration of the 2D map of strains collected at the midplane of the specimen is shown in Figure 5A,B in the crack growing and crack opening directions, respectively. These maps are in agreement in shape and dimensions with previous results presented in literature.[58,59] During the fatigue cycles applied in the X-ray diffraction test, slight positional corrections were applied to the sample in order to maintain its position with respect to the laboratory coordinate system. Hence, all the strain maps were obtained using the specimen boundaries as a reference, rather than laboratory equipment.

3 | METHODOLOGY FOR ESTIMATION OF THE PLASTIC ZONE

The estimation of the plastic zone starts by constructing the elastic component of the Von Mises equivalent strain map. The equivalent strain map is then used in combination with Hooke's law to generate the equivalent stress map around the crack tip. Finally, based on the yield strength, the stress map is thresholded to identify the boundaries of the plastic zone. Similar results can be obtained by thresholding the equivalent strain field instead of the equivalent stress field. Such an operation would use the strain representative of the yield strength. A summary of the different steps involved in the procedure is depicted as a flow diagram in Figure 6 shows that Young's modulus is used in the third step, and the yield strength was used in the fourth step. The experimental setup used at ID15 allowed only the crack growth and the crack opening components to be measured by X-ray diffraction (ε_{xx} and ε_{yy}, respectively). The experimental setup did not include the additional detectors required to measure other components. Consequently, the shear strain component (γ_{xy}) (Figure 7C) required for computing the Von Mises equivalent strain map was generated artificially by finite element modeling and hence was smoother than the other fields. A bidimensional model of the CT specimen was used considering symmetry along the crack plane. In order to capture the stress state of the midplane probed with synchrotron, plane strain conditions were adopted. The meshing was based on quadrilateral elements with nodes in the corners and in the middle of each side of the element. The meshing was very fine in the crack tip region with a minimum element size of $8 \times 8\ \mu m^2$. A total of 50,844 elements and 153,266 nodes were employed in the model. The symmetry condition inhibited the movement along the crack plane in the crack opening direction. In addition, the movement of last node ahead of the crack (in the ligament) was restricted both in the crack opening and crack growing direction, to avoid rigid body motion. The load was applied through the loading holes (see Figure 4) in the crack opening direction. Figure 7 depicts an example of application of this procedure and includes the contour plots of all fields employed in the methodology. Starting from the tensile

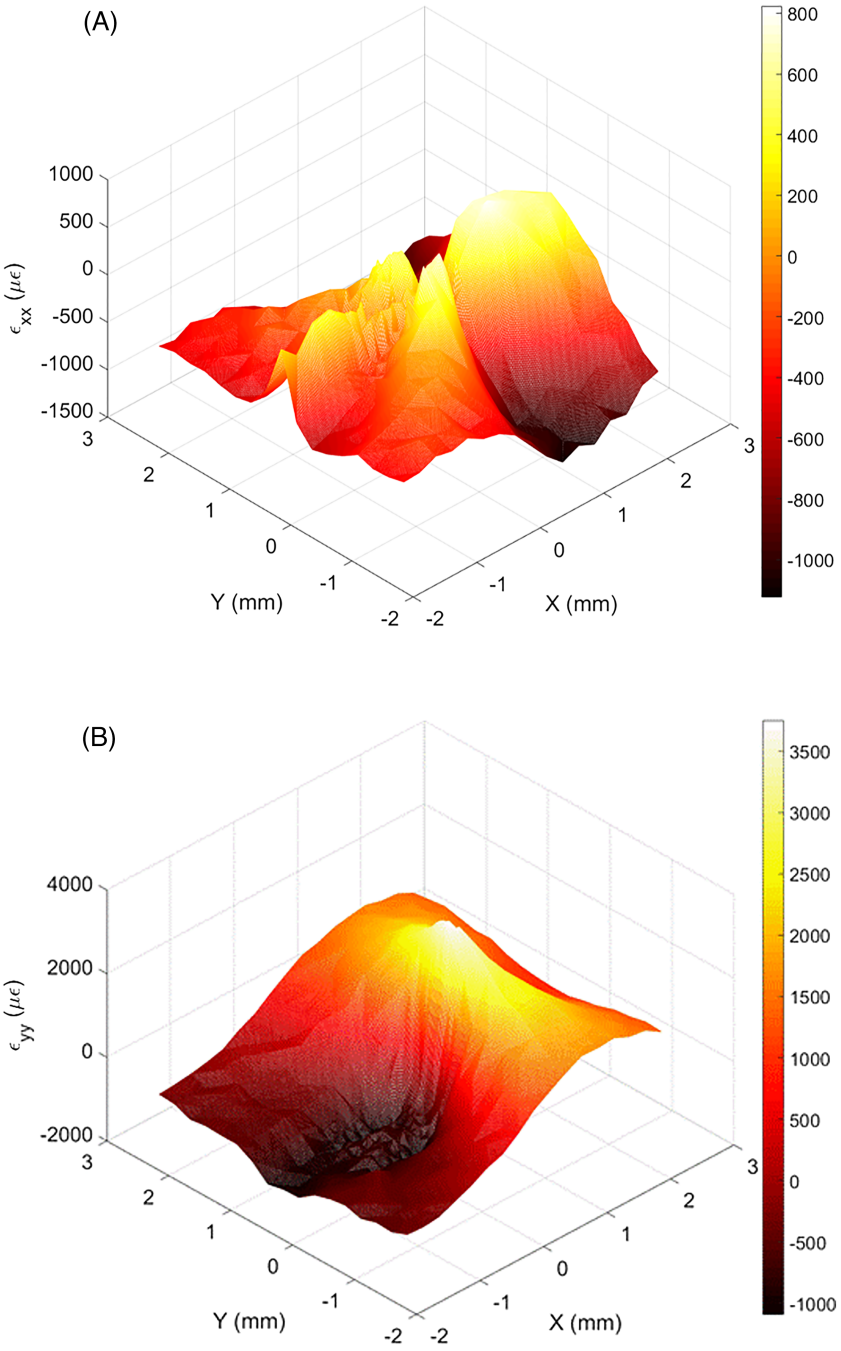

FIGURE 5 Strain fields (in 10^{-6}) obtained from X-ray diffraction data (A) along crack growing direction and (B) along crack opening direction. The crack tip is located at coordinates (0, 0) [Colour figure can be viewed at wileyonlinelibrary.com]

test, mechanical properties of the material are incorporated into the calculation algorithm. X-ray diffraction test previously presented contributes with the gridded maps of elastic strain surrounding the crack tip, both in crack growing and crack opening directions. The maps have been interpolated uniformly, in order to adjust the vertical and horizontal resolutions in both directions to the square root of the length of the domain. The shear strain map was also interpolated to present the same grid as the experimental fields.

The determination of the equivalent strain field, ε_{VM}, is based on the following expression[60]:

$$\varepsilon_{VM} = \beta\sqrt{(\varepsilon_{xx}-\varepsilon_{yy})^2+(\varepsilon_{yy}-\varepsilon_{zz})^2+(\varepsilon_{zz}-\varepsilon_{xx})^2+6\cdot\left[\left(\frac{\gamma_{xy}}{2}\right)^2+\left(\frac{\gamma_{yz}}{2}\right)^2+\left(\frac{\gamma_{zx}}{2}\right)^2\right]} \quad (2)$$

The β value depends upon the state of stress in the area of interest. Under plane strain conditions, ε_{zz}, γ_{xz}, γ_{yz} components are null, and so Equation 2 is largely simplified.

The thresholding process involves matching each point of the equivalent stress map against the yield strength of the material. Data points with values above the yield strength are considered plastically deformed.

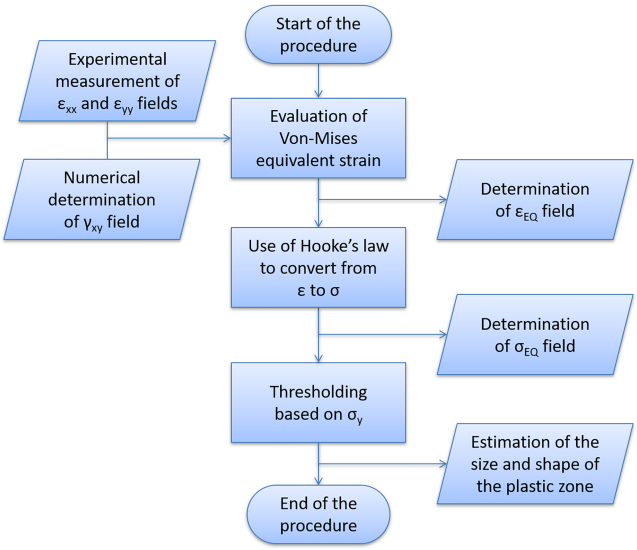

FIGURE 6 Flow diagram used to obtain the plastic zone from the strain maps obtained by X-ray diffraction [Colour figure can be viewed at wileyonlinelibrary.com]

The Von Mises criterion introduces the plane strain correction whereby the yield stress is shifted as a consequence of increasing constraint.[61] In order to estimate the size and shape of the plastic zone, the boundary obtained with the thresholding is analyzed with computational geometry with help of Delaunay triangulation.[62] Given a set S of random points in a 2D domain, Delaunay triangulation of S is a triangulation such that any point of S is inside the circumcircle of any triangle given. In the current application, S represents the area of the plastic zone. A point p is considered to be an α-extreme point in S if there exists a closed generalized disc of radius $\alpha_r = 1/\alpha$ which contains all points in S, and p lies on its boundary. Given two points p and q from S, they are considered α-neighbors if a closed generalized disc of radius $1/\alpha$ exists which contains all points of S, with both p and q in its boundary. Therefore, the α-shape of S is a graph whose vertices are α-extreme points and whose edges connect the respective α-neighbors.[63,64]

The area of the plastic zone is the result of applying Delaunay triangulation on the thresholded 2D map by taking into account all the pertinent triangles. Delaunay triangulation requires the parameter α_r to be manually adjusted (see Figure 8). Too large α_r parameter induces an excessive number of triangles to be considered within the plastic zone (Figure 8A,B), thus overestimating the plastic zone. An increasing number of triangles are discarded by reducing the value of α_r parameter since the disks generated by the algorithm become smaller and cannot circumscribe larger triangles. Selecting too small values of α_r parameter results in leaving triangles outside the relevant domain and generating two unconnected lobes (Figure 8D), thus underestimating the plastic zone. For the current situation, a trade-off can be achieved by reducing the value of α_r parameter to the point of having a standard butterfly shape of a plastic zone, where both lobes are connected (Figure 8C). In this work, α_r parameter values of 0.050 were chosen because produced the best results (Figure 8).

4 | RESULTS AND DISCUSSION

The results obtained from the algorithm's application to three fatigue stages are presented in Figure 9. For comparison purposes, Figure 9 also includes Westergaard's solution of the plastic zone under both plane stress and plane strain conditions.[61,65] The shape of the experimental plastic zone resembles a butterfly shape or a figure of eight, more in agreement with the plastic zone described by the theoretical plane strain curve. The cardioid shape typically observed under plane stress conditions[45,66] cannot be detected in the experimental plastic zone (Figure 9). This observation is in agreement with the majority of volume analyzed being at the midplane through the thickness or near that plane, where the state of stress is expected to be predominantly plane strain. A symmetry along the X-axis was observed for the three cases, in agreement with the load being of opening mode (mode I). Figure 9 also indicates that for all three cases studied, the experimental plastic zone is longer than the plane strain estimation based on Westergaard's solution and also narrower. Table 3 summarizes the size of the plastic zone (in mm^2) estimated with the help of Delaunay triangulation. Table 3 clearly shows an increment in the plastic zone size as the crack grows. This is expected since the nominal stress intensity factor was raised between stages FS1 and FS3.

Table 3 shows that the area of the experimental plastic zone is below that of plane strain for FS1. For the other two crack lengths (FS2 and FS3), the experimental plastic zone is in between the plane strain prediction and the plane stress prediction. In all cases, the experimental area is closest to the plane strain results. In terms of plastic zone size, this result is consistent with the largest portion of the material being probed at the midplane of a thick specimen. Nevertheless, it is worth mentioning that the volume analyzed contains more than one single plane, and so the plastic zone area is an average over different sections weighted towards the midplane.

The two main parameters that influence the state of stress are the thickness and the load level (stress intensity factor).[28,30] Increasing the thickness shifts the state towards plane strain conditions, while increasing the

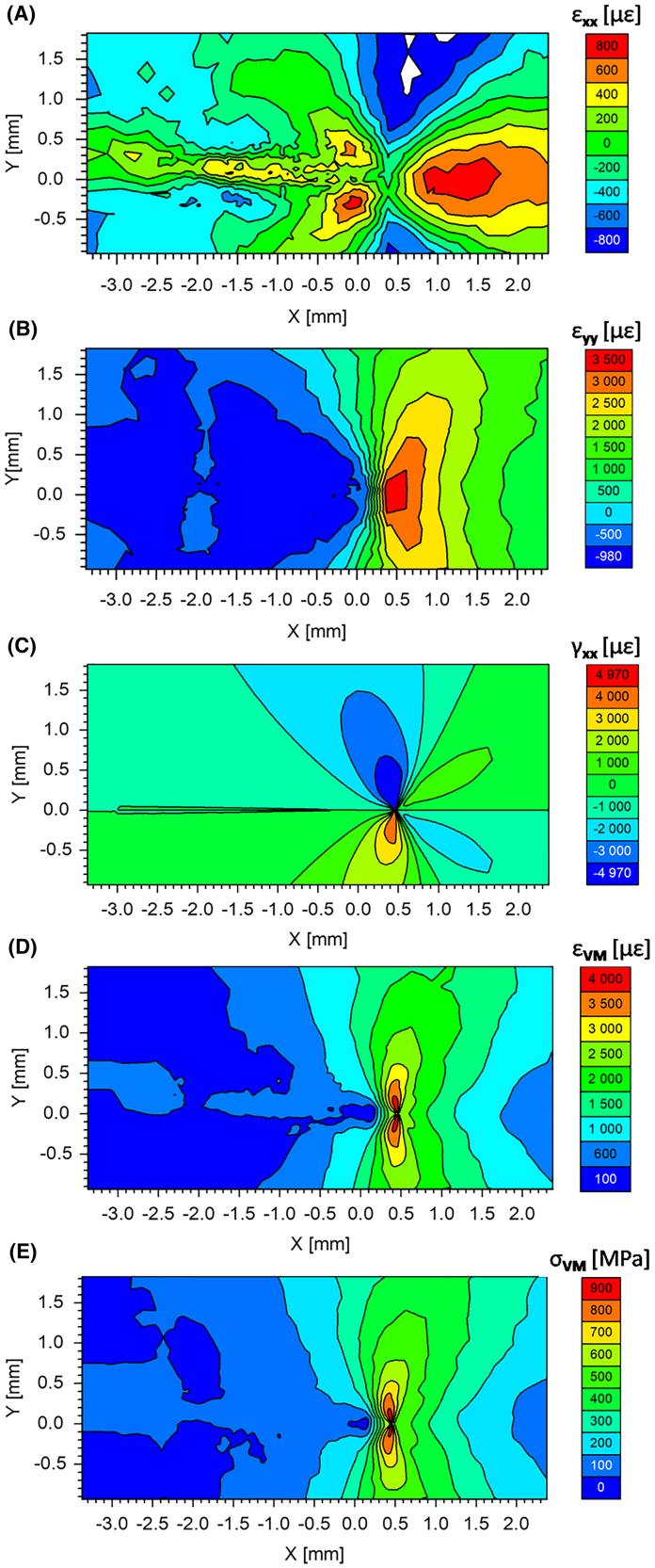

FIGURE 7 2D maps of stress or strain distributions around the crack tip for the fatigue stage FS3. (A) Normal strain field along crack growing direction (ε_{xx}). (B) Normal strain field along the crack opening direction (ε_{yy}). (C) Shear strain field (γ_{xy}). (D) Von Mises equivalent strain field. (E) Von Mises equivalent stress field. The crack tip is located at coordinates (0, 0) [Colour figure can be viewed at wileyonlinelibrary.com]

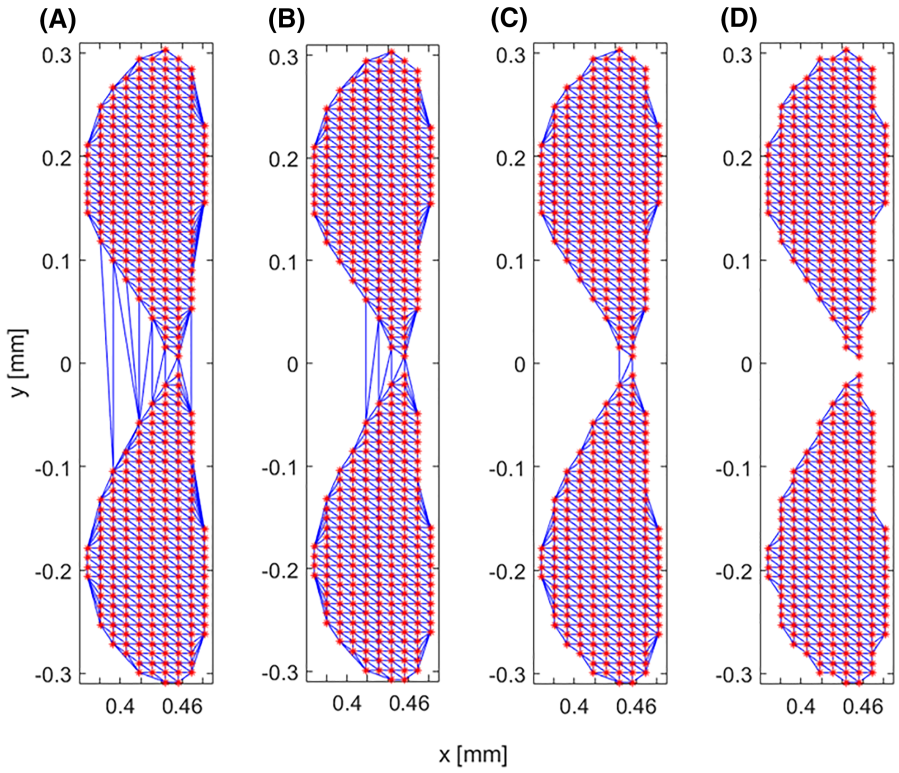

FIGURE 8 Examples of α-shapes of the domain S, given different αradii, α_r. From left to right: (A) $\alpha_r = 0.200$, (B) $\alpha_r = 0.100$, (C) $\alpha_r = 0.050$, (D) $\alpha_r = 0.015$ [Colour figure can be viewed at wileyonlinelibrary.com]

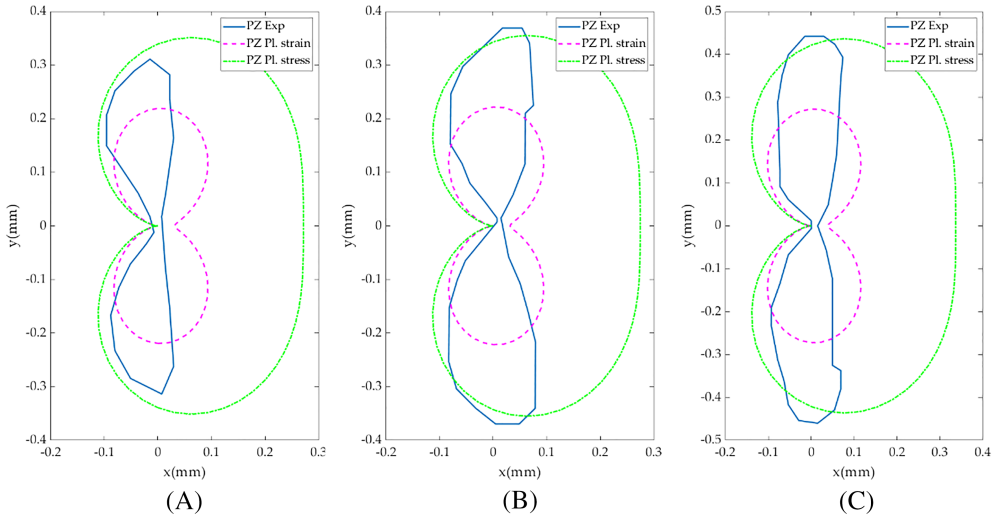

FIGURE 9 Plastic zones obtained and comparison with theoretical models of the plastic zone under plane strain and plane stress conditions at (A) fatigue stage 1 (FS1), (B) fatigue stage 2 (FS2), and (C) fatigue stage 3 (FS3) [Colour figure can be viewed at wileyonlinelibrary.com]

TABLE 3 Summary of the plastic zone areas for the three different fatigue stages

	FS1	FS2	FS3
Experimental (mm^2)	0.045	0.075	0.157
Plane strain (Westergaard) (mm^2)	0.059	0.061	0.091
Plane stress (Westergaard) (mm^2)	0.215	0.226	0.345

stress intensity factor shifts the conditions towards plane stress. In the current study, the thickness was kept constant and the stress intensity factor was increased. Accordingly, the state is expected to move away from plane strain and towards plane stress conditions. This swing away from plane strain conditions can also be observed by the fact that the experimental plastic zone clearly intersects the plane stress prediction in the two stages with higher load (FS2 and FS3), as seen in Figure 9. The plane stress influence on the plastic zone can also be observed in the asymmetry of the plastic zone along the vertical axis (Y axis in Figure 9). The increasing plane stress influence from FS1 to FS3 is also observed in Table 3. For FS1 with the lowest load level, the experimental plastic zone is closest to the plane strain plastic zone. For FS2 with intermediate load level, the

experimental plastic zone is still closest to the plane strain solution but is placed between the two states of stress. For FS3 with highest load level, the experimental plastic zone is clearly between both extremes, and the difference with respect the plane strain prediction increases.

Table 3 also allows a comparison with the early analytical models, including Rice, Irwin, Dugdale as well as others assuming a circular plastic zone that can be estimated according to the following:

$$r_p = \alpha \left(\frac{K}{\sigma_y} \right)^2 \tag{3}$$

where r_p is the plastic zone radius, K is the applied stress intensity factor, and σ_y is the yield strength. Each model used a different value for α correction factor.[16] Accordingly, the results shown in Table 3 can be used to estimate the correction factor. These are 0.027, 0.035, and 0.041 for fatigue stages FS1, FS2, and FS3, accordingly. The different models suggested correction factors ranging between 0.1 and 0.4 for different plane stress conditions and 0.05 for plane strain conditions.[16] They did not distinguish other stress state conditions in between these extreme conditions. The experimental estimation of the α correction factor is certainly closer to the plane strain figure given by the models. This is in agreement with our experiment being conducted under predominantly plane strain conditions. Differences between the results were expected since early models assumed a circular shape for the plastic zone,[67] and current models suggest that the shape of the plastic zone often has a butterfly or cardioid shape when conditions are closer to plane stress and a figure eight shape when conditions are close to plane strain.[68] Nevertheless, the gradual increase of the correction factor from FS1 to FS3 agrees with our previous discussion suggesting that conditions are much closer to plane strain and that, for the cases under study, increasing the stress intensity factor produces a slight shift towards plane stress.

5 | CONCLUSIONS AND FUTURE WORK

In this paper, a new procedure for estimation of the plastic zone deep inside opaque materials has been shown. The procedure is based on measuring 2D strain maps in the bulk of the material by means of synchrotron X-ray diffraction. The methodology has been applied to three different fatigue stages, and the plastic zone results have been compared with Westergaard's model for the plastic zone under plane strain and under plane stress conditions. The plastic zone measured with X-ray diffraction is more similar to that of plane strain conditions. This is due to the specimen having a considerable thickness (12 mm) and also due to the fact that most information is collected from the region at the midplane through the thickness. Accordingly, the state of the stress analyzed is predominantly under plane strain conditions. The experimental plastic zone lies between the plane strain and plane stress Westergaard's bounds. The observed plastic zone has a flatter shape, extending further from the crack plane in the crack opening direction and being less wide in the crack growing direction than theoretical predictions. The differences observed with increasing stress intensity factor suggest a slight shift towards plane stress but these being still predominantly plane strain conditions. New experiments are required to further investigate this issue. They should involve the following:

i. performing X-ray measurements at different positions through the thickness (in the current work, measurements were only taken at the mid-plane through the thickness of the specimen);
ii. reproducing these experiments with other X-ray configurations having more detectors so that other components, such as the shear strain can also be measured;
iii. analyzing different load frequencies and
iv. applying the methodology to different materials.

It is noteworthy that given the very limited availability of synchrotron facilities, progress on this field is necessarily slow. In addition, the current methodology might be improved by developing a 3D numerical model to estimate the shear component.

The results shown will be essential as a tool for accurate validation of 3D simulations. There exist an increasing number of works based on 3D modeling that have not been validated experimentally or have only been validated at the surface. Matching the material behaviour in the bulk, with results like the one presented here, in addition to the validations at the surface, is key to make the modeling reliable.

ACKNOWLEDGMENTS

We are grateful for the beam time granted by the ESRF (MA1483). We would also like to acknowledge the financial support of Programa Operativo FEDER (Junta de Andalucia, Spain) through grant reference UMA18-FEDERJA-250. This work was also supported by the Henry Royce Institute for Advanced Materials,

funded through EPSRC grants EP/R00661X/1, EP/S019367/1, EP/P025021/1, and EP/P025498/1 and the European Social Found, through the Youth Employment Initiative, grant reference UMAJI84. Industrial support from Bettergy SL and Dr Nicolas Ordonez is also greatly acknowledged, as well as access to different structures and materials in the energy industry. We are especially thankful to Dr. Thomas Buslaps (ESRF, France) for his help in the early stages of this study. We would also like to acknowledge funding for open access charge: Universidad de Malaga / CBUA.

AUTHOR CONTRIBUTION

Manuel Carrera: data treatment, visualization, writing, validation, and data curation. Alejandro S. Cruces: data treatment writing, conceptualization, visualization, validation, and investigation. Joseph F. Kelleher: writing, experimental testing, conceptualization, data curation, and review and editing. Yee-Han Tai: experimental testing, conceptualization, review and editing, and investigation. John R. Yates: writing, experimental testing, conceptualization, review and editing, and investigation. Philip J. Withers: writing, experimental testing, conceptualization, review and editing, and project administration. Pablo Lopez-Crespo: project administration, conceptualization, writing, validation, data curation, and review and editing.

DATA AVAILABILITY STATEMENT

The raw data and processed data required to reproduce these findings are available from the authors upon request.

ORCID

John R. Yates https://orcid.org/0000-0002-5888-8132
Pablo Lopez-Crespo https://orcid.org/0000-0002-5897-5615

REFERENCES

1. Pook LP. *Linear Elastic Fracture Mechanics for Engineers: Theory and Applications*. WIT Press; 2000.
2. Anderson TL. *Fracture Mechanics. Fundamentals and Applications*. Third ed. 2005.
3. Pommier S, Hammam R. Incremental model for fatigue crack growth based on a displacement partitioning hypothesis of mode I elastic-plastic displacement fields. *Fatigue Fract Eng Mater Struct*. 2007;30(7):582-598.
4. Lopez-Crespo P, Pommier S. Numerical analysis of crack tip plasticity and history effects under mixed mode conditions. *J Solid Mech Mater Eng*. 2008;2(12):1567-1576.
5. Christopher CJ, James MN, Patterson EA, Tee KF. A quantitative evaluation of fatigue crack shielding forces using photoelasticity. *Eng Fract Mech*. 2008;75(14):4190-4199.
6. James MN, Christopher CJ, Lu Y, Patterson EA. Local crack plasticity and its influences on the global elastic stress field. *Int J Fatigue*. 2013;46:4-15.
7. Vasco-Olmo JM, James MN, Christopher CJ, Patterson EA, Díaz FA. Assessment of crack tip plastic zone size and shape and its influence on crack tip shielding. *Fatigue Fract Eng Mater Struct*. 2016;39(8):969-981.
8. Antunes FV, Rodrigues SM, Branco R, Camas D. A numerical analysis of CTOD in constant amplitude fatigue crack growth. *Theor Appl Fract Mech*. 2016;85:45-55.
9. Antunes FV, Serrano S, Branco R, Prates P. Fatigue crack growth in the 2050-T8 aluminium alloy. *Int J Fatigue*. 2018;115:79-88.
10. Vasco-Olmo JM, Díaz Garrido FA, Antunes FV, James MN. Plastic CTOD as fatigue crack growth characterising parameter in 2024-T3 and 7050-T6 aluminium alloys using DIC. *Fatigue Fract Eng Mater Struct*. 2020;43(8):1719-1730.
11. Antunes FV, Ferreira MSC, Branco R, Prates P, Gardin C, Sarrazin-Baudoux C. Fatigue crack growth versus plastic CTOD in the 304L stainless steel. *Eng Fract Mech*. 2019;214:487-503.
12. Lopez-Crespo P, Moreno B, Susmel L. Influence of crack tip plasticity on fatigue propagation. *Theor Appl Fract Mech*. 2020;108:102667.
13. Suresh S. *Fatigue of Materials*. 2nded. New York, USA: Cambridge University Press; 1998.
14. Hutchinson JW. Plastic stress and strain fields at a crack tip. *J Mech Phys Solids*. 1968;16(5):337-347.
15. Paris P, Erdogan F. A critical analysis of crack propagation laws. *J Basic Eng*. 1963;85(4):528-533.
16. Kujawski D, Ellyin F. On the size of plastic zone ahead of crack tip. *Eng Fract Mech*. 1986;25(2):229-236.
17. Banerjee S. Influence of specimen size and configuration on the plastic zone size, toughness and crack growth. *Eng Fract Mech*. 1981;15(3–4):343-390.
18. Park HB, Kim KM, Lee BW. Plastic zone size in fatigue cracking. *Int J Press Vessel pip*. 1996;68(3):279-285.
19. Wu SC, Xu ZW, Yu C, Kafka OL, Liu WK. A physically short fatigue crack growth approach based on low cycle fatigue properties. *Int J Fatigue*. 2017;103:185-195.
20. Xin G, Hangong W, Xingwu K, Liangzhou J. Analytic solutions to crack tip plastic zone under various loading conditions. *Eur J Mech a/Solids*. 2010;29(4):738-745.
21. Banks TM, Garlick A. The form of crack tip plastic zones. *Eng Fract Mech*. 1984;19(3):571-581.
22. Camas D, Lopez-Crespo P, Gonzalez-Herrera A, Moreno B. Numerical and experimental study of the plastic zone in cracked specimens. *Eng Fract Mech*. 2017;185:20-32.
23. Sivaneri NT, Xie YP, Kang BSJ. Elastic-plastic crack-tip-field numerical analysis integrated with moire interferometry. *Int J Fract*. 1991;49(4):291-303.
24. McClung RC. Crack closure and plastic zone sizes in fatigue. *Fatigue Fract Eng Mater Struct*. 1991;14(4):455-468.
25. Zhang JZ, Zhang JZ, Yi Du S. Elastic-plastic finite element analysis and experimental study of short and long fatigue crack growth. *Eng Fract Mech*. 2001;68(14):1591-1605.
26. Lopez-Crespo P, Camas D, Antunes FV, Yates JR. A study of the evolution of crack tip plasticity along a crack front. *Theor Appl Fract Mech*. 2018;98:59-66.

27. Besel M, Breitbarth E. Advanced analysis of crack tip plastic zone under cyclic loading. *Int J Fatigue.* 2016;93:92-108.
28. Yue J, Dong Y, Guedes Soares C. An experimental-finite element method based on beach marks to determine fatigue crack growth rate in thick plates with varying stress states. *Eng Fract Mech.* 2018;196:123-141.
29. Marques LFN, Meggiolaro MA, de CJTP, Martha LF. Elastoplastic 3D analyses of plastic zone size dependencies on load-to-yield strength and on crack size-to-width ratios under mixed mode I/II. *Theor Appl Fract Mech.* 2020;107:102490.
30. Camas D, Garcia-Manrique J, Gonzalez-Herrera A. Numerical study of the thickness transition in bi-dimensional specimen cracks. *Int J Fatigue.* 2011;33(7):921-928.
31. Gustafson S, Ludwig W, Shade P, et al. Quantifying microscale drivers for fatigue failure via coupled synchrotron X-ray characterization and simulations. *Nat Commun*. 2020;11(1):1-10.
32. Steuwer A, Edwards L, Pratihar S, et al. In situ analysis of cracks in structural materials using synchrotron X-ray tomography and diffraction. *Nucl Instruments Methods Phys Res Sect B Beam Interact with Mater Atoms*. 2006;246(1):217-225.
33. Croft M, Zhong Z, Jisrawi N, et al. Strain profiling of fatigue crack overload effects using energy dispersive X-ray diffraction. *Int J Fatigue.* 2005;27(10–12):1408-1419.
34. Lopez-Crespo P, Peralta JV, Withers PJ. Synchrotron X-ray diffraction based method for stress intensity factor evaluation in the bulk of materials. *Theor Appl Fract Mech*. 2018;98:72-77.
35. Steuwer A, Rahman M, Shterenlikht A, Fitzpatrick ME, Edwards L, Withers PJ. The evolution of crack-tip stresses during a fatigue overload event. *Acta Mater*. 2010;58(11):4039-4052.
36. Lopez-Crespo P, Steuwer A, Buslaps T, et al. Measuring overload effects during fatigue crack growth in bainitic steel by synchrotron X-ray diffraction. *Int J Fatigue.* 2015;71:11-16.
37. Salvati E, Zhang H, Fong KS, Song X, Korsunsky AM. Separating plasticity-induced closure and residual stress contributions to fatigue crack retardation following an overload. *J Mech Phys Solids*. 2017;98:222-235.
38. Simpson CA, Kozuki S, Lopez-Crespo P, Mostafavi M, Connolley T, Withers PJ. Quantifying fatigue overload retardation mechanisms by energy dispersive X-ray diffraction. *J Mech Phys Solids*. 2019;124:392-410.
39. Davidson DL, Lankford J, Yokobori T, Sato K. Fatigue crack tip plastic zones in low carbon steel. *Int J Fract.* 1976;12(4):579-585.
40. Khor KH, Buffiére JY, Ludwig W, Sinclair I. High resolution X-ray tomography of micromechanisms of fatigue crack closure. *Scr Mater*. 2006;55(1):47-50.
41. Barabash R, Gao Y, Sun Y, et al. Neutron and X-ray diffraction studies and cohesive interface model of the fatigue crack deformation behavior. *Philos Mag Lett*. 2008;88(8):553-565.
42. Lopez-Crespo P, Peralta JV, Kelleher JF, Withers PJ. In situ through-thickness analysis of crack tip fields with synchrotron X-ray diffraction. *Int J Fatigue*. 2019;127:500-508.
43. Lopez-Crespo C, Cruces AS, Seitl S, Moreno B, Lopez-Crespo P. Estimation of the plastic zone in fatigue via micro-indentation. *Materials (Basel)*. 2021;14.
44. Hutař P, Náhlík L, Knésl Z. The effect of a free surface on fatigue crack behaviour. *Int J Fatigue.* 2010;32(8):1265-1269.
45. Sousa RA, Figueiredo FP. The principle of similitude analysed from plastic zones estimates ahead crack tips. *Int J Mech Sci*. 2014;89:403-412.
46. Matvienko YG. The effect of out-of-plane constraint in terms of the T-stress in connection with specimen thickness. *Theor Appl Fract Mech.* 2015;80:49-56.
47. Garcia-Manrique J, Camas D, Gonzalez-Herrera A. Study of the stress intensity factor analysis through thickness: Methodological aspects. *Fatigue Fract Eng Mater Struct*. 2017;40(8):1295-1308.
48. Huang X, Liu Y, Dai Y. Characteristics and effects of T-stresses in central-cracked unstiffened and stiffened plates under mode I loading. *Eng Fract Mech.* 2018;188:393-415.
49. Matvienko YG. The effect of crack-tip constraint in some problems of fracture mechanics. *Eng Fail Anal*. 2020;110:104413.
50. Gardin C, Fiordalisi S, Sarrazin-Baudoux C, Petit J. Numerical simulation of fatigue plasticity-induced crack closure for through cracks with curved fronts. *Eng Fract Mech.* 2016;160:213-225.
51. Croft M, Jisrawi N, Ignatov A, Holtz RL, Zhong Z. Fatigue crack growth "overload effect": Mechanistic insights from in-situ synchrotron measurements. *J Strain Anal Eng Des*. 2012;47(2):83-94.
52. Zhang W, Simpson CA, Lopez-Crespo P, et al. The effect of grain size on the fatigue overload behaviour of nickel. *Mater Des*. 2020;189:108526.
53. Robertson IM. Measurement of the effects of stress ratio and changes of stress ratio on fatigue crack growth rate in a quenched and tempered steel. *Int J Fatigue.* 1994;16(3):216-220.
54. Lopez-Crespo P, Withers PJ, Yusof F, et al. Overload effects on fatigue crack-tip fields under plane stress conditions: Surface and bulk analysis. *Fatigue Fract Eng Mater Struct*. 2012;36(1):75-84.
55. Kelleher JF, Lopez-Crespo P, Yusof F, Withers PJ. The use of diffraction to study fatigue crack tip mechanics. *Mater Sci Forum*. 2010;652:216-221.
56. Korsunsky AM, Baimpas N, Song X, et al. Strain tomography of polycrystalline zirconia dental prostheses by synchrotron X-ray diffraction. *Acta Mater*. 2011;59(6):2501-2513.
57. Lopez-Crespo P, Mostafavi M, Steuwer A, Kelleher JF, Buslaps T, Withers PJ. Characterisation of overloads in fatigue by 2D strain mapping at the surface and in the bulk. *Fatigue Fract Eng Mater Struct*. 2016;39(8):1040-1048.
58. Steuwer A, Santisteban JR, Turski M, Withers PJ, Buslaps T. High-resolution strain mapping in bulk samples using full-profile analysis of energy-dispersive synchrotron X-ray diffraction data. *J Appl Cryst*. 2004;37(6):883-889.
59. Croft M, Shukla V, Jisrawi NM, et al. Mapping and load response of overload strain fields: Synchrotron X-ray measurements. *Int J Fatigue.* 2009;31(11–12):1669-1677.
60. Bannantine JA, Comer JJ, Handrock JL. *Fundamentals of Metal Fatigue Analysis*.1990.
61. Broek D. *Elementary Engineering Fracture Mechanics*.1982.
62. Delaunay B. Sur la sphère vide. A la mémoire de Georges Voronoï. *Bull lAcadémie des Sci lURSS Cl des Sci mathématiques*. 1934;793-800.

63. Akkiraju N, Edelsbrunner H, Facello M, Fu P, Mücke EP, Varela C. Alpha shapes: Definition and software. *Proc 1st Int Comput Geom Softw Work*. 1995;63-66.
64. Cazals F, Giesen J, Pauly M, Zomorodian A. Conformal alpha shapes. *Proceedings Eurographics/IEEE VGTC Symposium Point-Based Graphics*. 2005;55-61.
65. Westergaard HM. Bearing pressures and cracks cylinder, and related problems of cracks. *J Appl Mech*. 2021;6:A49-A53.
66. Torabi AR, Shahbazian B. Notch tip plastic zone determination by extending Irwins model. *Theor Appl Fract Mech.* 2020;108: 102643.
67. Ewalds HL, Wanhill RJH. *Fracture Mechanics*. Butterwort; 1984.
68. de Castro JTP, Meggiolaro MA. *Fatigue Design Techniques: Vol. III - Crack Propagation*. CreateSpac; 2016.

How to cite this article: Carrera M, Cruces AS, Kelleher JF, et al. Characterisation of the crack tip plastic zone in fatigue via synchrotron X-ray diffraction. *Fatigue Fract Eng Mater Struct*. 2022; 45(7):2086-2098. doi:10.1111/ffe.13705